Electronic Supplementary Material (ESI) for RSC Advances.

Support information

Preparation of Co-N Carbon Nanosheets Oxygen Electrode Catalyst by Controlled Crystallization of Cobalt Salt Precursors for All-Solid-State Al-air Battery

Jianhua Shen,[a] Lu Meng,[a] Yanyan Liu,[a] Cheng Chen,[b] Yihua Zhu*,[a] and Chunzhong Li*[a]

[a] Key Laboratory for Ultrafine Materials of Ministry of Education, School of Materials Science and Engineering, East China University of Science and Technology, Shanghai 200237, China

[b] School of Environmental and Materials Engineering, College of Engineering, Shanghai Polytechnic University, Shanghai 201209, China
E-mail: yhzhu@ecust.edu.cn; czli@ecust.edu.cn;

Experimental

Chemicals

P123 (Aldrich, $EO_{20}PO_{70}EO_{20}$, Ma=5800), Nafion (5 wt%), RuO_2 and MWCNTs were obtained from Sigma-Aldrich. Pt/C (20 wt%) was obtained from Johnson-Matthey. Cyanamide 50% w/w aqueous solution was obtained from Alfa Aesar. All other chemicals were purchased from Shanghai Lingfeng Chemical Reagent Co. Ltd. All chemicals are of analytical grade and used as received without further purification. Ultrapure water (18 MΩ·cm) was used for all experiments.

Other material synthesis

Melamine (0.75 g), metal salt precursors ($Fe(NO_3)_3 \cdot 9H_2O$, $CoCl_2 \cdot 6H_2O$, $C_4H_6O_4Co \cdot 4H_2O$, $CoSO_4 \cdot 7H_2O$, 0.42 mmol), PEO-PPO-PEO (P123, 0.5 g) and ultrapure water (15 mL) were stirred about 2 h at room temperature. Then the solution was dried under 80 ^oC to remove water. The dried precursor was placed into a crucible and heated up to 500 ^oC to form metal-functionalized carbon nitride, subsequently, then heated to 800 ^oC with the rate of 3 $^oC\ min^{-1}$ for 2 h in N_2 atmosphere. Unstable and inactive species are removed from the heat-treated samples via pre-leach in 0.5 M H_2SO_4 at 80 ^oC for 24 h.

Materials characterization

Scanning electron microscopy (FE-SEM: S-4800, equipped with an energy dispersive X-ray analyzer (EDX).) and Transmission electron microscopy (TEM: JEM-2100, operated at 200 kV) were used to examine the morphology and microstructure of all samples. The wide-angle X-ray diffraction ((RIGAK, D/MAX 2550 VB/PC, Japan) was used for powderanalysis. The Co content was measured by thermogravimetric analysis (SDT-Q600 simultaneous TGA/DSC thermogravimetric analyzer). The specific surface area, pore volume, and pore size of samples were investigated by Bruauer-Emmett-Teller (BET) and Barrett-Joyner-Halenda (BJH) models. Raman spectra were recorded with a Bruker RFS 100/S spectrometer. X-ray photoelectron spectroscopy obtained with VG ESCA 2000 with a magnesium anode was used to demonstrate the content and the doping types of carbon, nitrogen and metal contents. All data were corrected using the C1s peak at 284.8 eV as an internal standard.

ORR measurement. The cyclic voltammogram experiments were conducted in O_2-saturated 0.1 M KOH solution for ORR with the scan rate of 10 mV s^{-1} at room temperature. The linear sweep voltammograms were performed in the O_2-saturated 0.1 M KOH solution at rotation speed varying from 225 to 1600 rpm and with the scan rate of 10 mV s^{-1}. The stability tests were performed in O_2-saturated 0.1 M KOH at room temperature before and after 3000 cycles at a sweep rate of 100 mV s^{-1}. At the end of the cycles, the resulting electrodes were used for polarization curves at a sweep rate of 10 mV s^{-1}. The number of electrons (n) involved in the ORR can be calculated from the Koutecky-Levich (K-L) equation:

$$\frac{1}{J} = \frac{1}{J_L} + \frac{1}{J_K} = \frac{1}{B\omega^{1/2}} + \frac{1}{J_K} \quad (1)$$

$$B = 0.2nFC_0(D_0)^{2/3}v^{-1/6} \quad (2)$$

Where J is the measured current density, J_L and J_K are the diffusion- and kinetic-limiting current densities. B is Levich slope which is given by (2). n is the number of electrons transferred for ORR. ω is the rotation speed in rpm. F is the Faraday constant (96485 C mol^{-1}). ν is the kinetic viscosity (0.01 cm^2 s^{-1}) and D_0 is the diffusion coefficient of O_2 in 0.1 M KOH (1.9×10^{-5} cm^2 s^{-1}). Bulk concentration of oxygen C_0 is 1.2×10^{-6} mol cm^{-3}.

OER measurement. OER tests were conducted in O_2-saturated 0.1 M KOH electrolyte with the scan rate of 10 mV s^{-1} at room temperature. The potential range was from 1.0 to 1.9 V (vs. RHE). All data were corrected using the *E–iR* relation, where *i* is the current and *R* is the uncompensated electrolyte ohmic resistance, which was obtained *via* high-frequency AC impedance. The stability was evaluated by chronamperometry test at 1.62V (vs RHE) with rotation rate of 1600 rpm.

Calculation method. Plane-wave density functional theory (DFT) + U calculations of the electronic properties of the electrocatalysts were performed using the CASTEP module in Material Studio. GGA with PBE functional was used for the DFT exchange correlation energy, and 300 eV of kinetic energy cutoff was assigned to the plane-wave basis set. The self-consistent field (SCF) tolerance was 2×10^{-6} eV. The Brillouin zone was sampled by 1×1×1 k-points. The core electrons were replaced with

ultrasoft pseudo-potentials. To module the Co-N/CNs electrocatalyst, a Co-N_3 site is embedded in a periodic 5×5×1 graphene. The vacuum spacing is set to more than 20 Å along the surface normal to avoid the interactions between images. To compare the electrocatalytic reactivity between Co-N_3 site and Co particles, an isolated octahedral Co_6 cluster was also built to model the Co particles. The binding energy was calculated by subtracting the energies of the isolated adsorbate and the catalyst from the total energy of the adsorbed system.

The ORR four electron reaction path mechanism was divided into four elementary steps[1]:

$$* + O_2 + H_2O(l) + e^- \rightarrow HOO* + OH^- \quad (1)$$

$$HOO* + e^- \rightarrow O* + OH^- \quad (2)$$

$$O* + H_2O(l) + e^- \rightarrow HO* + OH^- \quad (3)$$

$$HO* + e^- \rightarrow OH^- + * \quad (4)$$

in which * indicates the adsorption site and the steps (1)–(4) corresponded to the four-electron transfer processes.

The OER four electron reaction path mechanism was showed as follows[2]:

$$H_2O(l) + * \rightarrow HO* + H^+ + e^- \quad (5)$$

$$HO* \rightarrow O* + H^+ + e^- \quad (6)$$

$$O* + H_2O(l) \rightarrow HOO* + H^+ + e^- \quad (7)$$

$$HOO* \rightarrow O_2 + * + H^+ + e^- \quad (8)$$

Based on these mechanisms, the Gibbs free energy change of basic reaction of (1)-(8) are calculated as follows.

The free energy of OH^- is calculated by $G_{OH^-} = G_{H_2O(l)} - G_{H^+}$ and $G_{H^+} + \mu_{e^-} = \frac{1}{2} G^{\theta}_{H_2} - eU + k_bT\ln(a_{H^+})$.

$$\Delta G_1 = G_{HOO*} - G_* - G_{O_2(g)} - \frac{1}{2} G^{\theta}_{H_2} + eU - k_bT\ln(a_{H^+}) \quad (9)$$

$$\Delta G_2 = G_{O*} - G_{HOO*} + G_{H_2O(l)} - \frac{1}{2}G^{\theta}_{H_2} + eU - k_bT\ln(a_{H^+}) \quad (10)$$

$$\Delta G_3 = G_{HO*} - G_{O*} - \frac{1}{2}G^{\theta}_{H_2} + eU - k_bT\ln(a_{H^+}) \quad (11)$$

$$\Delta G_4 = G_{*} - G_{HO*} + G_{H_2O(l)} - \frac{1}{2}G^{\theta}_{H_2} + eU - k_bT\ln(a_{H^+}) \quad (12)$$

ΔG_{O*}, ΔG_{HO*}, ΔG_{HOO*} are defined as follows:

$$\Delta G_{HOO*} = G_{HOO*} - G_{*} - [2G_{H_2O(l)} - 1.5G_{H_2(g)}] \quad (13)$$

$$\Delta G_{O*} = G_{O*} - G_{*} - [G_{H_2O(l)} - G_{H_2(g)}] \quad (14)$$

$$\Delta G_{HO*} = G_{HO*} - G_{*} - [G_{H_2O(l)} - 0.5G_{H_2(g)}] \quad (15)$$

Since the high-spin ground state of oxygen can't be accurately described by DFT calculations, the experimental value of the formation energy of water is adopted to calculate the free energy of oxygen.

$$\Delta G_w = G_{H_2O(l)} - G_{H_2(g)} - 0.5G_{O_2(g)} = -2.46\ eV \quad (16)$$

So the free energy change could be calculated by the follows:

$$\Delta G_1 = \Delta G_{HOO*} + 2\Delta G_w + eU - k_bT\ln(a_{H^+}) \quad (17)$$

$$\Delta G_2 = \Delta G_{O*} - \Delta G_{HOO*} + eU - k_bT\ln(a_{H^+}) \quad (18)$$

$$\Delta G_3 = \Delta G_{HO*} - \Delta G_{O*} + eU - k_bT\ln(a_{H^+}) \quad (19)$$

$$\Delta G_4 = -\Delta G_{HO*} + eU - k_bT\ln(a_{H^+}) \quad (20)$$

$$\Delta G_5 = -\Delta G_4 \quad (21)$$

$$\Delta G_6 = -\Delta G_3 \quad (22)$$

$$\Delta G_7 = -\Delta G_2 \quad (23)$$

$$\Delta G_8 = -\Delta G_1 \quad (24)$$

The first step in the free energy diagram became uphill as the potential increases was regarded as the determining step in the ORR mechanism; Similarly, the first step in the free energy diagram became uphill as the potential decreases was regarded as the

determining step in the OER mechanism[3,4]. Furthermore, the overpotential was defined as the difference between the fore-men,tioned potential and equilibrium potential, given as:

$$\eta_{ORR} = \max\{\Delta G_1, \Delta G_2, \Delta G_3, \Delta G_4\}/e + 1.23\ V \quad (25)$$

$$\eta_{OER} = \max\{\Delta G_5, \Delta G_6, \Delta G_7, \Delta G_8\}/e - 1.23\ V \quad (26)$$

For each step, the reaction free energy ΔG is defined as the difference between free energies of the initial and final states and is given by the expression,

$$\Delta G = \Delta E + \Delta ZPE - T\Delta S + eU - k_b T \ln(a_{H^+}) \quad (27)$$

where ΔE is the reaction energy of reactant and product molecules adsorbed on catalyst surface, obtained from DFT calculations, where T is the temperature and ΔS is the entropy change. For the zero-point energy (ZPE), the vibrational frequencies of adsorbed species (O*, OH*, and OOH*) were calculated to obtain ZPE contribution in the free energy expression.

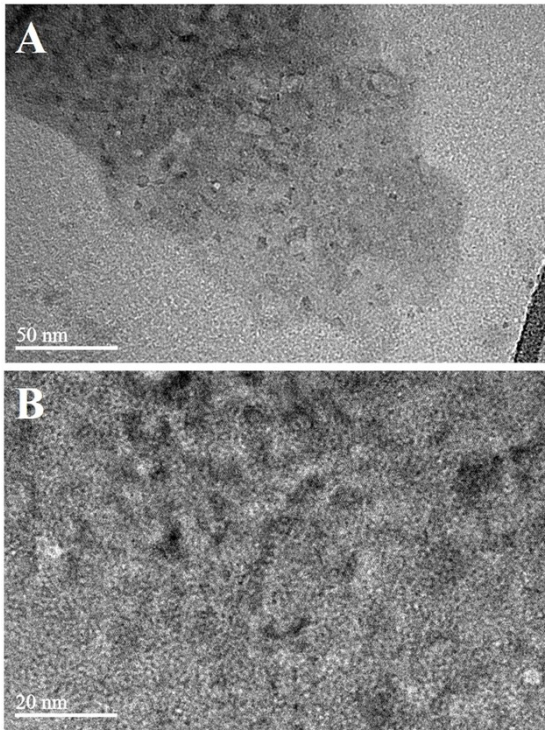

Fig. S1. TEM images of Co-N/CNs-800.

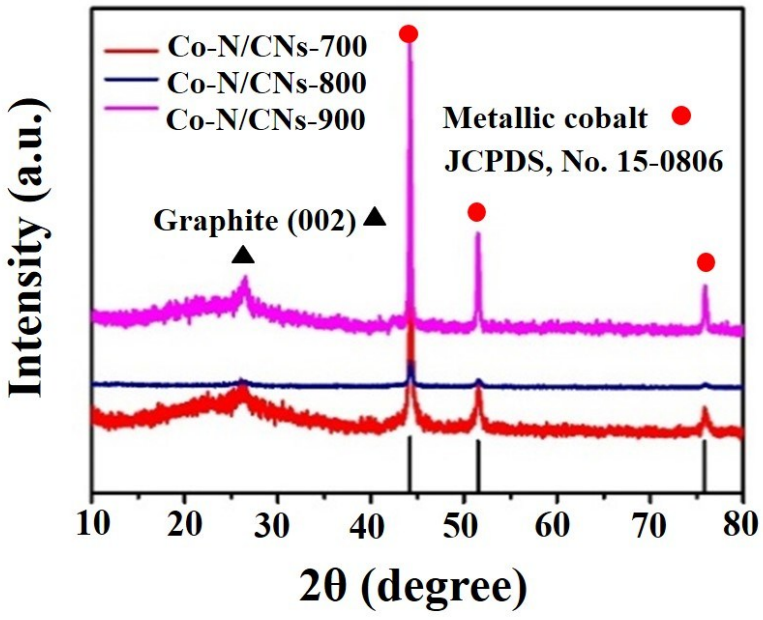

Fig. S2. Typical XRD patterns of Co-N/CNs.

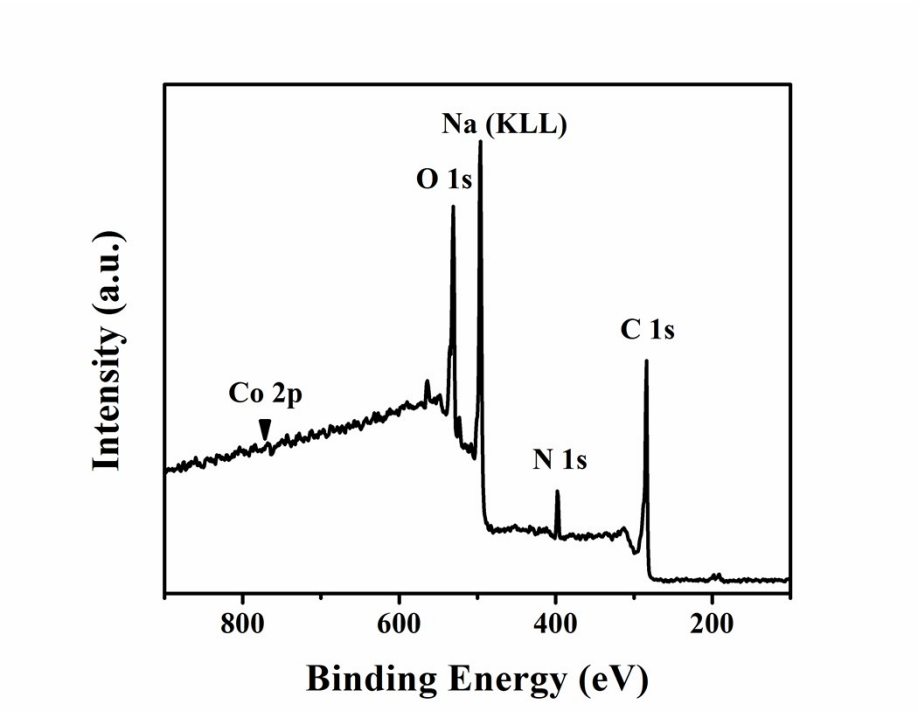

Fig. S3. General XPS spectrum of Co-N/CNs-800.

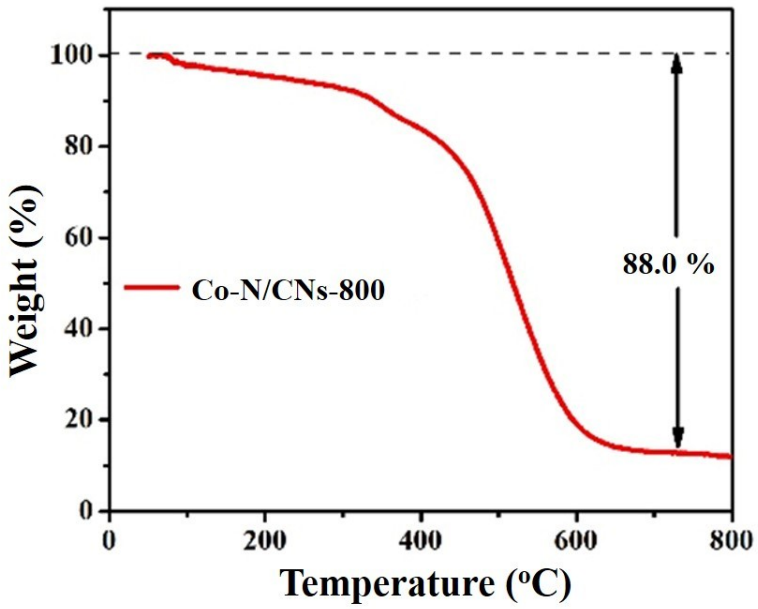

Fig. S4. TGA curve of Co-N/CNs-800 measured from 25 to 800 °C in atmospheric air with a heating rate of 10 °C min^{-1}.

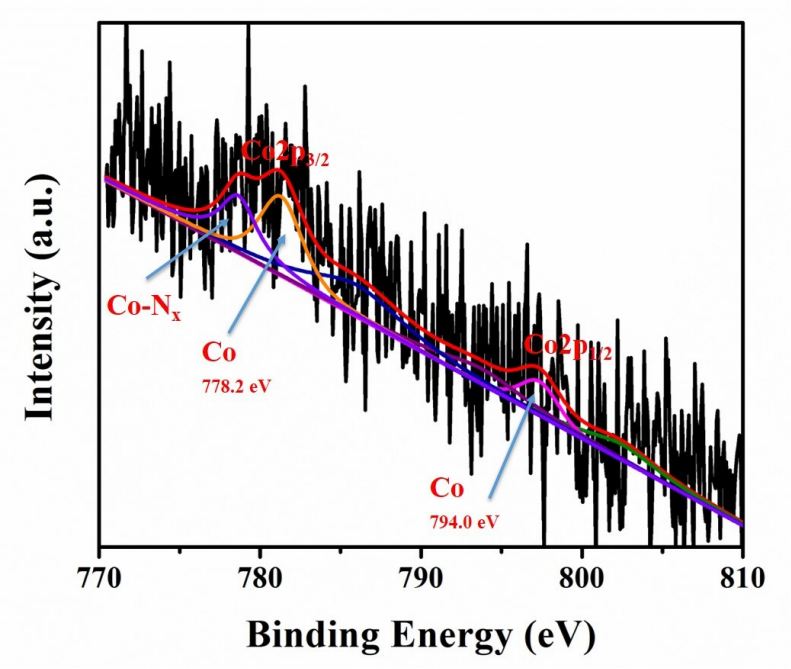

Fig. S5. High resolution Co 2p spectra of Co-N/CNs-800.

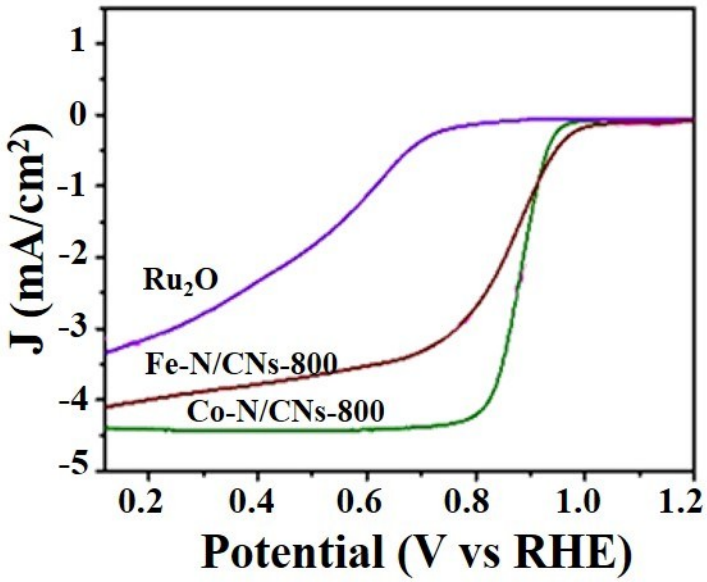

Fig. S6. LSV curves of Co-N/CNs-800, Fe-N/CNs-800 and RuO_2 at a rotation rate of 1600 rpm with a scan rate of 10 mV s^{-1}.

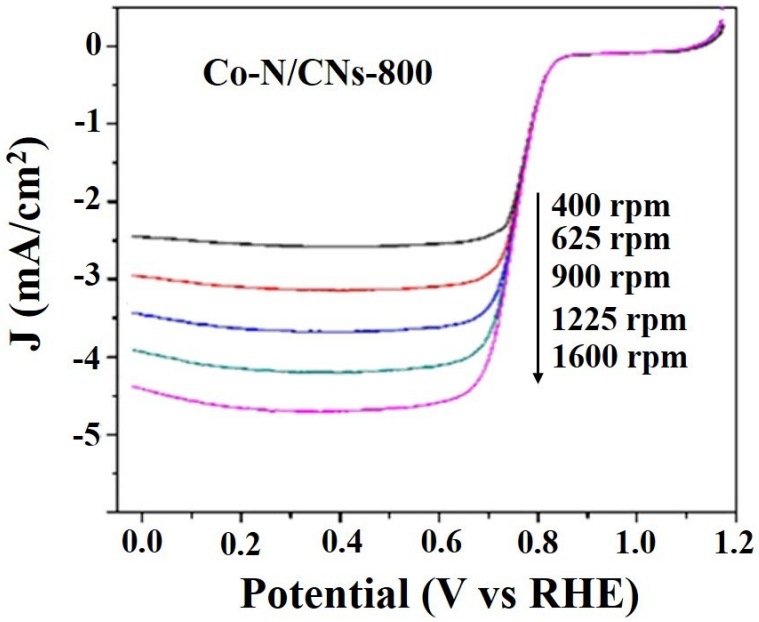

Fig. S7. LSV curves of Co-N/CNs-800 catalyst with different rotation rates at a scan rate of 10 mV s^{-1}.

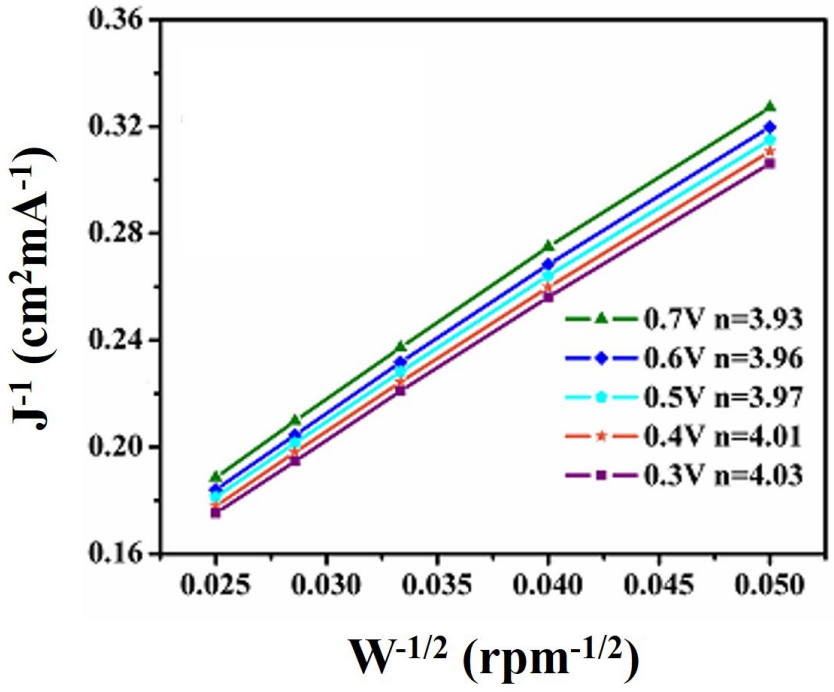

Fig. S8. K–L plots of Co-N/CNs-800 catalyst obtained from the RDE results.

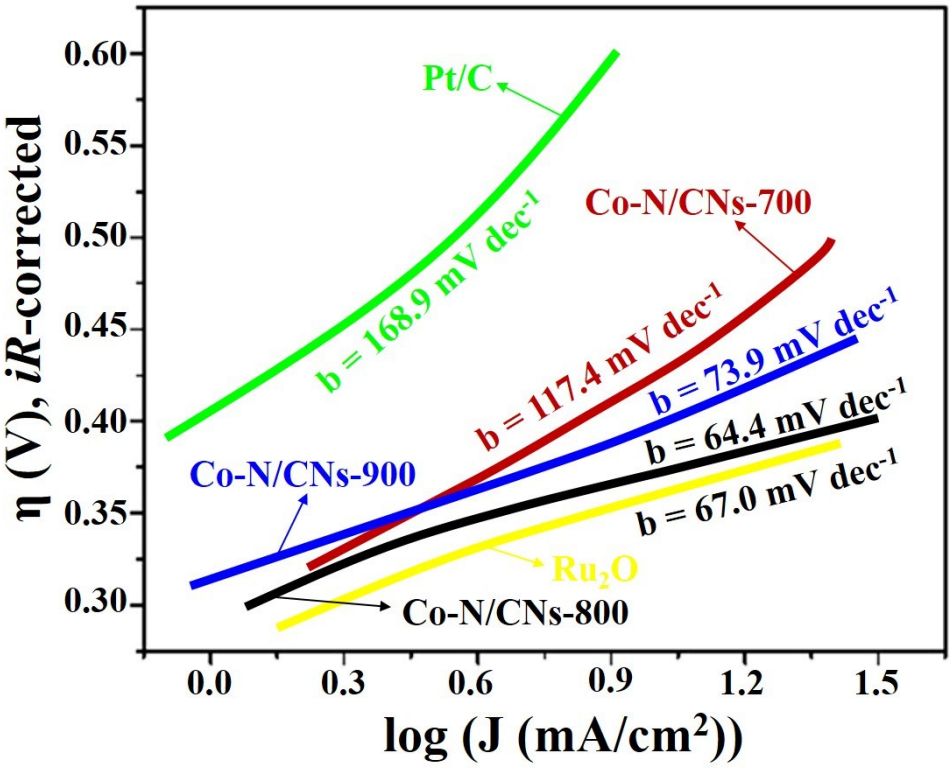

Fig. S9. Tafel plots of all catalysts from the polarization curves.

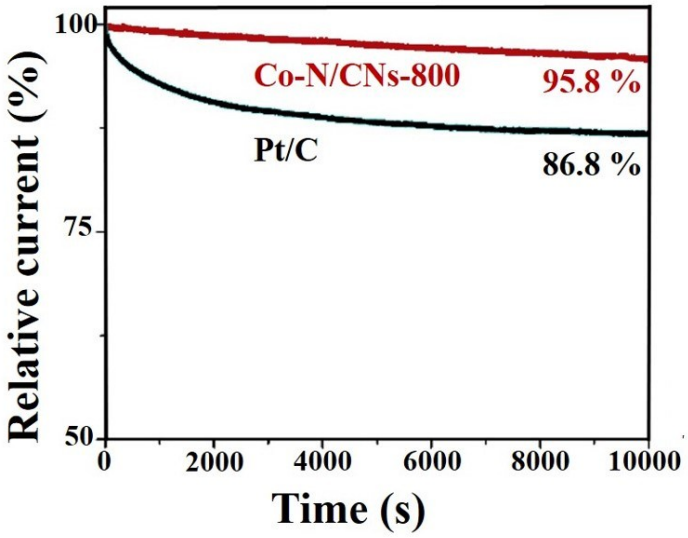

Fig. S10. *I–t* plots of Co-N/CNs-800 and Pt/C at -0.4 V in O_2-saturated 0.1 M KOH.

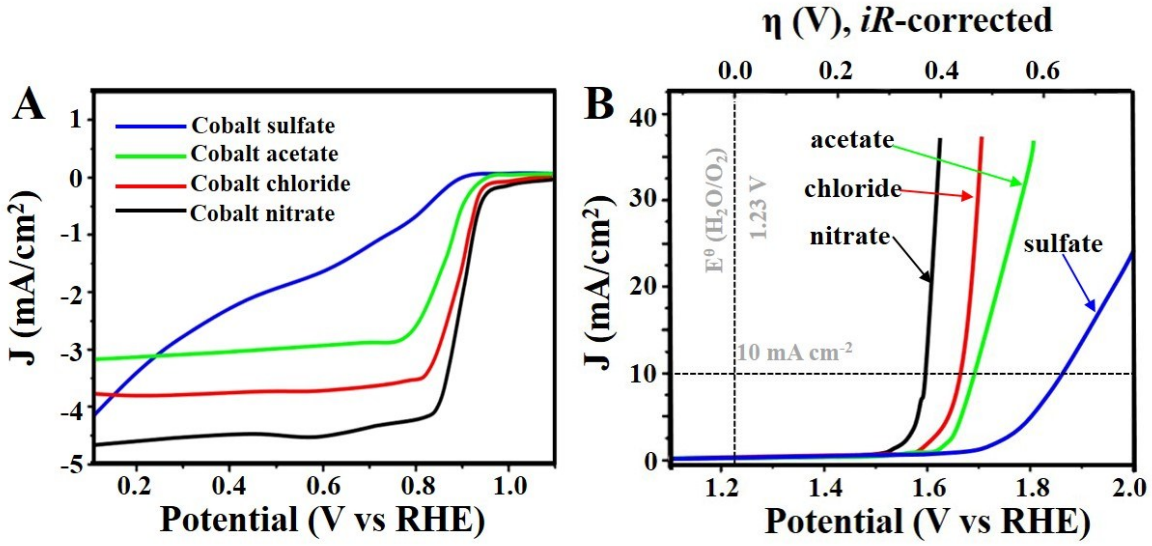

Fig. S11. RDE LSV curves (A) and polarization curves (B) of Co-N/CNs with different cobalt precursors.

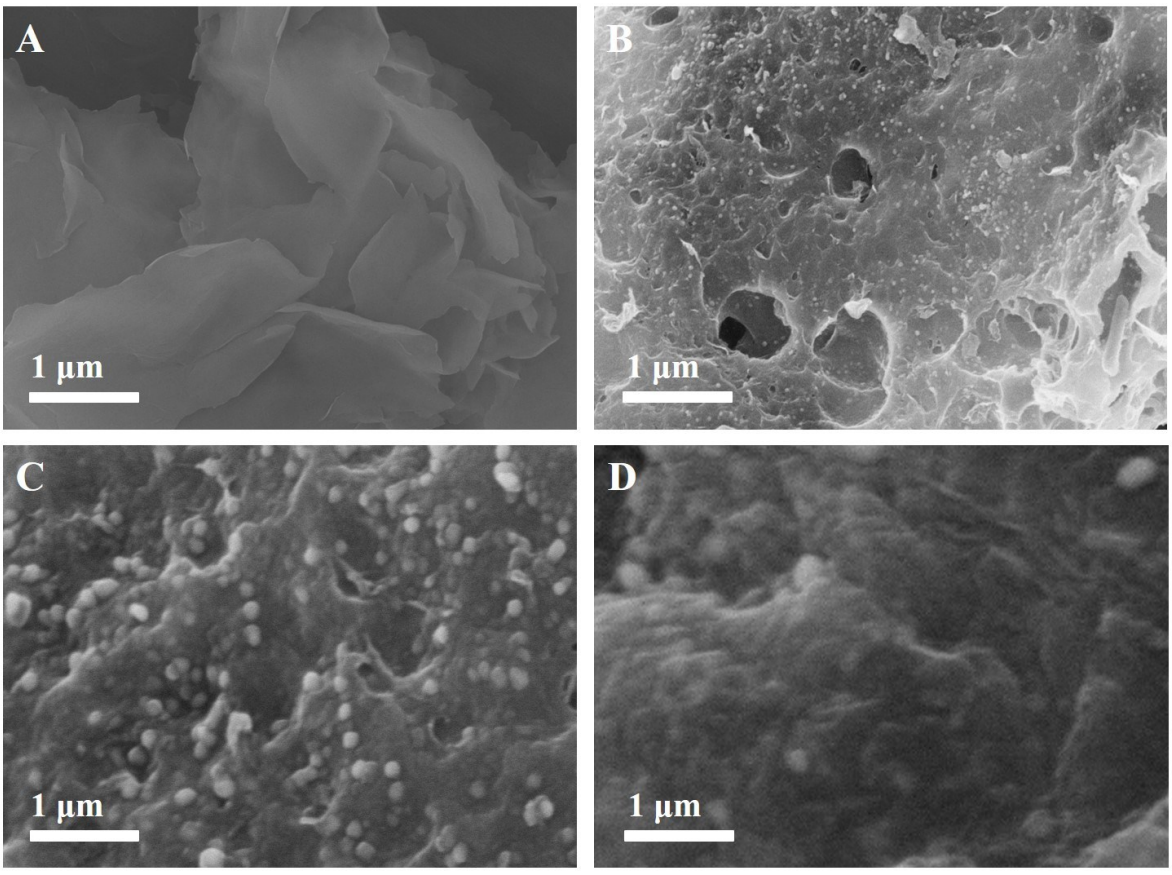

Fig. S12. SEM images of Co-N/CNs with different cobalt precursors (A) nitrate, (B) chloride, (C) acetate and (D) sulfate.

The overall free energy change, ΔG, is the sum of the free energy due to the formation of a new volume and the free energy due to the new surface created. For spherical particles

$$\Delta G = -\frac{4}{V}\pi r^3 k_B T \ln(S) + 4\pi r^2 \gamma \qquad (1)$$

where V is the molecular volume of the precipitated species, r is the radius of the nuclei, k_B is the Boltzmann constant, S is the saturation ratio, and γ is the surface free energy per unit surface area. When $S > 1$, ΔG has a positive maximum at a critical size, r^*.

$$r^* = \frac{2V\gamma}{3k_B T \ln(S)} \qquad (2)$$

This maximum free energy is the activation energy for nucleation. Nuclei larger than the critical size will further decrease their free energy for growth and form stable nuclei that grow to form particles. The critical nuclei size r^* can be obtained by setting $d\Delta G/dr = 0$.

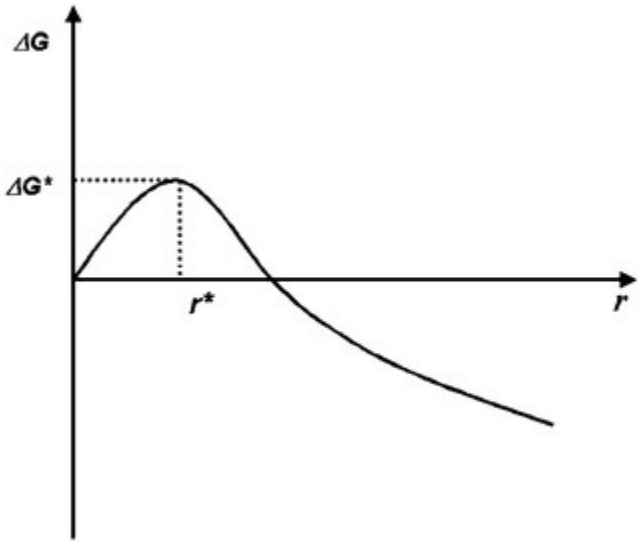

Fig. S13. Illustration of the overall free energy ΔG as a function of the growth particle size r. [5]

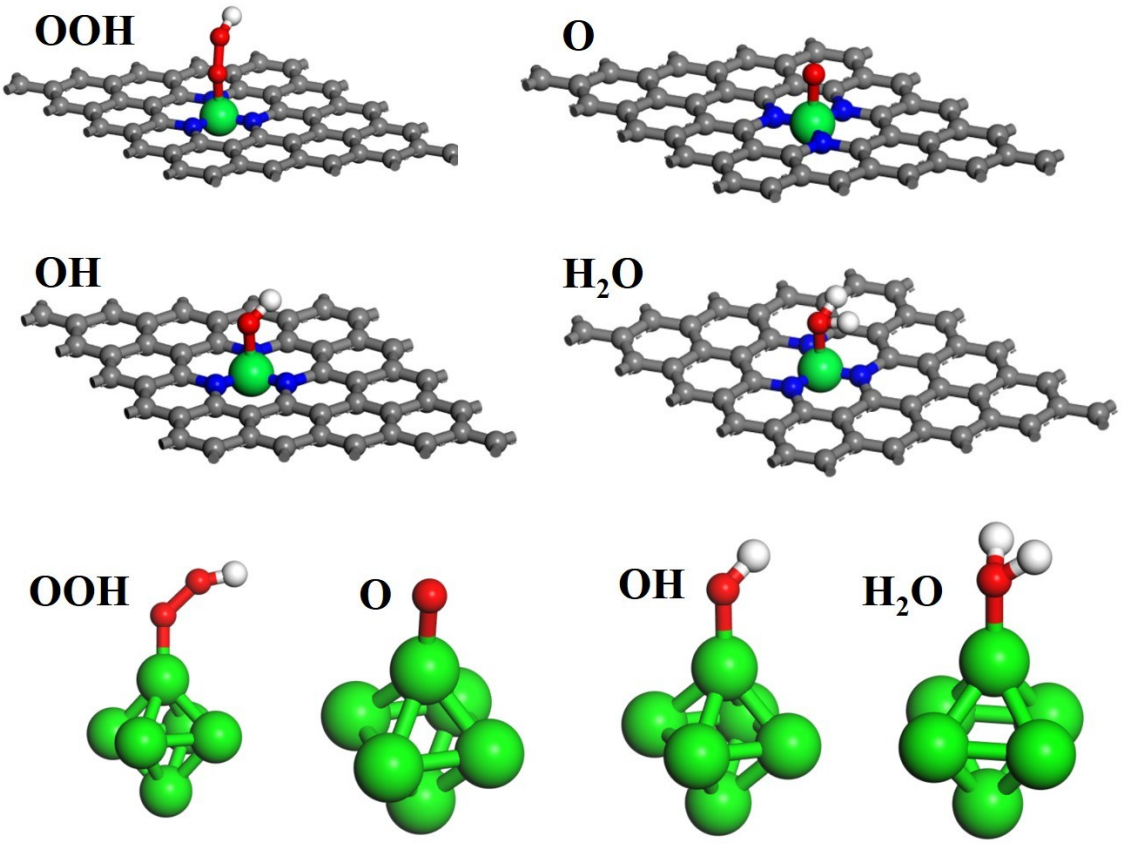

Fig. S14. Configurations of adsorbates on Co-N/CNs and Co nanoparticles.

Table S1. Comparison of ORR and OER activity parameters with reported bifunctional electrocatalysts.

Catalyst	Catalyst Loading (mg cm^{-2})	$E_{J-3,\,ORR}$ (V)	$E_{J10,\,OER}$ (V)	ΔE ($E_{J10,\,OER}$-$E_{J-3,\,ORR}$)	Ref.
CNT@NCNT	0.25	0.70	1.76	1.06	6
S/N_Fe-27	0.80	0.87	1.78	0.91	7
Co/N-C-800	0.25	0.74	1.60	0.86	8
Mn-Oxide	0.50	0.73	1.77	1.04	9
N-graphene/CNT	0.88	0.69	1.65	0.96	10
$La_{0.3}$-5582	0.639	0.59	1.63	1.04	11
20 wt% IrO_2/C	N.A.	0.73	1.60	0.87	11
20 wt% Pt/C	N.A.	0.86	2.02	1.16	11
20 wt% Ir/C	0.25	0.59	1.64	1.05	12
Co-N/CNs-800	0.20	0.74	1.58	0.84	This work

Table S2. Specific values of Co-N/CNs with different cobalt precursors.

	OER overpotentials ɳ (V)	ORR half-wave potential (V)	ORR onset potential (V)	Size of Co NPs in carbon sheets (nm)	Water solubility (mol/L)	
					20 °C	80 °C
Cobalt nitrate	0.39	0.89	0.98	5.6	3.44	8.97
Cobalt chloride	0.44	0.87	0.97	32.9	2.12	6.63
Cobalt acetate	0.47	0.85	0.96	80.7	1.54	3.24
Cobalt sulfate	0.62	0.45	0.92	100.8	1.29	2.49

Table S3. Atomic Concentration Table from XPS

	C 1s	N 1s	Co 2p3
Atomic ratio	89.24	10.68	0.09

References for Supporting Information

[1] Y. Jiao, Y. Zheng, M. Jaroniec, S. Z. Qiao, *J. Am. Chem. Soc.* **2014**, *136*, 4394.

[2] I. C. Man, H. Y. Su, F. Calle-Vallejo, H. A. Hansen, J. I. Martínez, N. G. Inoglu, J. Kitchin, T. F. Jaramillo, J. K. Nørskov, J. Rossmeisl, *ChemCatChem* **2011**, *3*, 1085.

[3] J. Rossmeisl, A. Logadottir, J. K. Nørskov, *Chem. Phys.* **2005**, *319*, 178.

[4] J. Rossmeisl, Z. W. Qu, H. Zhu, G. J. Kroes, J. K. Nørskov, *J. Electroanal. Chem.* **2007**, *607*, 83.

[5] C. Burda, X. B. Chen, R. Narayanan and M. A. El-Sayed, *Chem. Rev.* **2005**, *105*, 1025.

[6] G. L. Tian, Q. Zhang, B. Zhang, Y. G. Jin, J. Q. Huang, D. S. Su, F. Wei, *Adv. Funct. Mater.* **2014**, *24*, 5956.

[7] N. R. Sahraie, J. P. Paraknowitsch, C. Göbel, A. Thomas, P. Strasser, *J. Am. Chem. Soc.* **2014**, *136*, 14486.

[8] Y. H. Su, Y. H. Zhu, H. L. Jiang, J. H. Shen, X. L. Yang, W. J. Zou, J. D. Chen, C. Z. Li, *Nanoscale* **2014**, *6*, 15080.

[9] J. Seo, D. Cha, K. Takanabe, J. Kubotaad, K. Domen, *Phys. Chem. Chem. Phys.* **2013**, *16*, 895.

[10] Z. H. Wen, S. Q. Ci, Y. Hou, J. H. Chen, *Angew. Chem. Int. Ed.* **2014**, *53*, 6496.

[11] J. I. Jung, H. Y. Jeong, J. S. Lee, M. G. Kim, J. Cho, *Angew. Chem. Int. Ed.* **2014**, *53*, 4582.

[12] C. Tang, H.-F. Wang, X. Chen, B.-Q. Li, T.-Z. Hou, B. Zhang, Q. Zhang, M.-M. Titirici, F. Wei, *Adv. Mater.* **2016**, *28*, 6845.